

## Flux Determination through Ultra High Energy Muons by Using Pair-Meter Technique

Sharda Pandey\* and Satendra K Chauhan

Department of Physics, University of Lucknow, Lucknow-226007, Uttar Pradesh, India

### Abstract

The cosmic ray spectrum exhibits two transition regions. The steepening of the spectrum occurs around 106 GeV known as knee region and the flattening of the spectrum occurs around 109 GeV known as ankle region. The reason of this transition in cosmic ray spectrum is not known. When the cosmic rays interact with the atmospheric nuclei they produce muons. The decay of long live  $d$  mesons at GeV energies contributes to the conventional muon fluxes. At higher energies, some contribution to the fluxes of muons will come from the interactions of short lived particles with the atmospheric nuclei. This contribution will give rise to prompt muon fluxes. In order to understand the prompt contribution to the neutrino and muon fluxes, we have selected high energy (TeV) muons for our studies. The dominant processes for this energy range are pair production and bremsstrahlung. For this energy region, we are using pair-meter technique to achieve a reliable reconstruction of the muon energies. Here we are taking a detector with dimensions  $15.6\text{ m} \times 15.6\text{ m} \times 78\text{ m}$  and which is placed 705 m underground from the surface of the earth. This study will help us to understand the contribution of prompt muon fluxes in higher energy region. It will also help us in understanding the possible compositional changes in the cosmic ray spectrum.

**Keywords:** Cosmic ray muons; Pair-meter technique; Ultra-high energy cosmic ray

### Introduction

Cosmic rays are free source of elementary particles and have enormous range of energies, still they produce small amount of striking rate at the detector level. Uncontrollable fluxes have been produced, which is the major disadvantage of cosmic rays. The study of cosmic ray spectrum enhances our knowledge about both astrophysics and particle physics [1-5], and also gives a signature of the existence of the new particles and some physics behind it, which was confirmed by some accelerator experiments. These experiments provide us to understand the structure of matter and interaction between its building blocks. The interaction of high energy cosmic rays with the earth's atmospheric nuclei produces extensive air showers, which are continuously rains on the earth through all the directions. These extensive air showers have been generated by the following interactions-

- Electromagnetic interactions of charged particles, which gives electrons and photons.
- Inelastic hadronic interactions, which gives the secondary fluxes of particles.
- Nuclear interactions, which gives the compositional changes between chemical and isotropic composition of cosmic ray nuclei.

Here we consider hadronic interactions only and focus on to determine the muon fluxes, generated from the decay of produced secondary hadrons. The range of cosmic ray energy lies some eV to 1020 eV and its spectrum obeys a power law behaviour of differential flux where the value of spectral index  $\gamma = 2.7$  at knee and  $\gamma = 3.1$  beyond knee. This behaviour changes at two points in the spectrum [6-11].

1. The steepening of the spectrum known as knee region occurs at energy  $\approx 106\text{ GeV}$ .
2. The flattening of the spectrum known as ankle region occurs at energy  $\approx 109\text{ GeV}$ .

This type of changes in the transition at knee and ankle is highly intriguing and not clear to understand because the ground array

experiments do not give a reliable reconstruction of the energy. This problem can be solved by taking two ways. The first way to study about the generation of some new heavy particles at knee energy and the second way to measure the compositional change of primary cosmic rays at knee energy. Here we have adopted the first way. Pair-meter technique for the measurement of muon energy is useful for the large iron detectors. This technique provides a reliable reconstruction of muon energy and energy resolution is not affected with the increase in muon energy.

### Pair-meter technique

This technique is useful for large size iron detectors and by means of which one can measure the individual muon energy. This technique is not useful for the small size detectors. Since muons have the high penetrating power ability due to their massive nature, therefore for the energy measurement, it requires some different technique from other particles which provides a better resolution of energy measurement of muons this technique also provides the measurement of frequency as well as energy of electron and positron pair production produced by high energy muons traversed in dense matter. The energy measurement process includes-

1. The differential cross section of pair production and bremsstrahlung processes are generated by muon of energy  $E_{\mu}$  above a threshold  $E_0$ .

\*Corresponding author: Sharda Pandey, Department of Physics, University of Lucknow, Lucknow-226007, Uttar Pradesh, India, Tel: 088086 15285; E-mail: [sharda2012536@gmail.com](mailto:sharda2012536@gmail.com)

Received February 14, 2017; Accepted March 24, 2017; Published March 29, 2017

Citation: Pandey S, Chauhan SK (2017) Flux Determination through Ultra High Energy Muons by Using Pair-Meter Technique. J Astrophys Aerospace Technol 5: 140. doi:10.4172/2329-6542.1000140

Copyright: © 2017 Pandey S, et al. This is an open-access article distributed under the terms of the Creative Commons Attribution License, which permits unrestricted use, distribution, and reproduction in any medium, provided the original author and source are credited.

2. A relative energy transfer above threshold,  $v = E_0/E_\mu$ , where  $E_0$  is threshold energy and  $E_\mu$  is muon energy above threshold.

3. Calculation of energy loss for each cascade resulting from Bremsstrahlung and Pair production.

4. Inferring the muon energy with the help of total number of cascades at detector having energies above a threshold  $E_0$ .

### Pair production cross section

The differential pair production cross section can be calculated by taking some approximation of relative energy transfer and threshold energy is given by [4,5,12,13].

$$v = \frac{E_0}{E_\mu} \ll \frac{2me}{m\mu} \quad (1)$$

$$E_0 \gg 2m_e 189\sqrt{e}Z^{1/3} \approx 0.3Z^{1/3}\text{GeV} \quad (2)$$

where  $m_e$  is the mass of electron,  $e$  the electron charge and  $Z$  is the atomic number. Here we are taking  $Z = 26$  for the iron nuclei. Therefore, the differential cross-section of pair-production process through muon is [12].

$$v \frac{d\sigma}{dv} \approx \frac{14\alpha}{9\pi t_0} \ln\left(\frac{kmeE_\mu}{E_0m_\mu}\right) \quad (3)$$

Where a fine structure constant and  $k = 1.8$  and  $t_0$  is the radiation length (rl).

The radiation length is the average amount of matter for both pair production and bremsstrahlung energy loss. The general form of expression of radiation length is:

$$t_0 = \left[ \frac{4N_{av}Z(Z+1)}{A} \alpha r_e^2 \ln\left(189Z^{-1/3}\right) \right]^{-1} \quad (4)$$

Approximate values of  $t_0$  can be calculated by the Hayakawa formula [14].

$$t_0 \approx 10^3 \frac{A}{6Z(Z+1)} \text{gcm}^{-2} \quad (5)$$

where  $N_{av}$  is Avogadro number,  $r_e$  classical electron radius and  $A$  is the Atomic weight for iron nuclei ( $A=56$ ).

Therefore, the radiation length is [6]  $t_0 = 13.75 \text{ g cm}^{-2}$

The Figure 1 shows the behaviour of differential cross-section of pair production and brems strahlung above the threshold energy  $E_0$ . The integral cross-section of pair production is:

$$\sigma(E_0, E_\mu) \approx \frac{7\alpha}{9\pi t_0} \left( \ln^2\left(\frac{kmeE_\mu}{E_0m_\mu}\right) + C \right) \quad (6)$$

Where correction term  $C \approx 1.4$  [14].

### Bremsstrahlung cross section

The brems strahlung is the process in which the interaction of charged particles with the electromagnetic field of atomic nuclei produces photons. The expression of differential cross-section for bremsstrahlung is given by:

$$v \frac{d\sigma}{dv} = 4\alpha r^2 \left[ \{ (1-y) + y^2 \} \{ Z^2 (L_{rad} - f(z)) + Z'_{rad} \} \right] \quad (7)$$

$$L_{rad}(z) = \ln(184.15Z^{-1/3}) \text{ for } Z \geq 5 \quad (8)$$

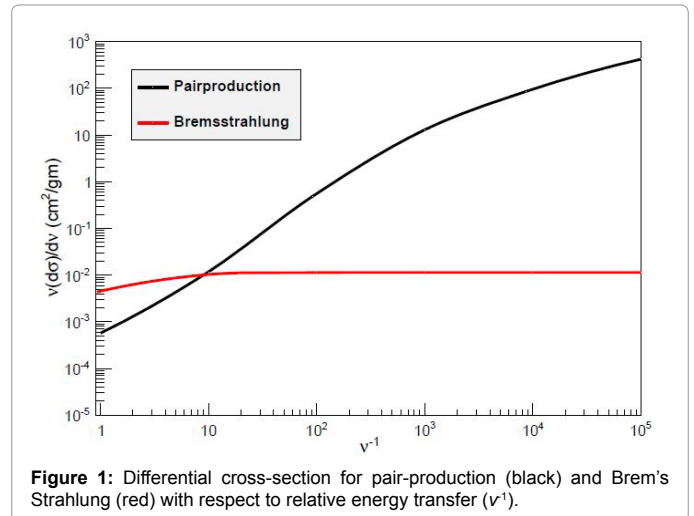


Figure 1: Differential cross-section for pair-production (black) and Brem's Strahlung (red) with respect to relative energy transfer ( $v^{-1}$ ).

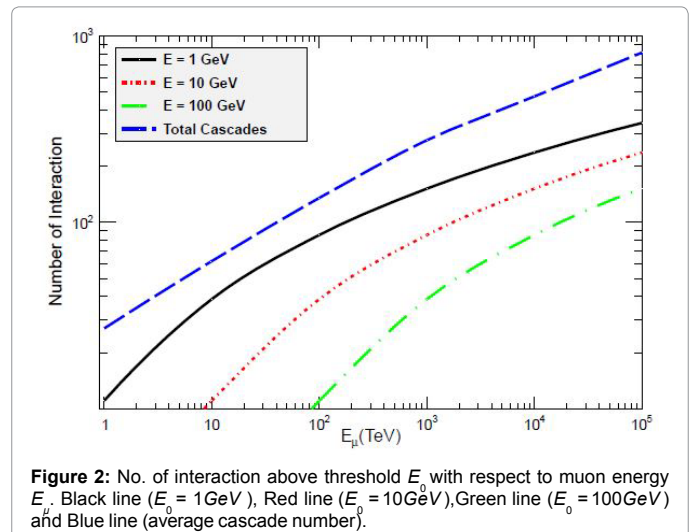


Figure 2: No. of interaction above threshold  $E$  with respect to muon energy  $E_\mu$ . Black line ( $E_0 = 1\text{ GeV}$ ), Red line ( $E_0 = 10\text{ GeV}$ ), Green line ( $E_0 = 100\text{ GeV}$ ) and Blue line (average cascade number).

$$L'_{rad}(z) = \ln(1194Z^{-2/3}) \text{ for } Z \geq 5 \quad (9)$$

$f(z)$  is coulomb correction function. The integral cross section of bremsstrahlung:

$$\sigma_{br} = \frac{4}{3} \frac{1}{n_a t_0} \ln\left(\frac{E_\mu}{E_0}\right) \quad (10)$$

### Number of interactions of muons

The number of interaction of muons can be calculated by the total cross-section of pair production as well as bremsstrahlung, which gives the total number of cascades of muons ( $M$ ).

For pair production process the total number of cascades above the threshold energy  $E_0$  can be calculated by:

$$M = T t_0 \sigma(E_\mu, E_0) \quad (11)$$

$$M \approx T t_0 \frac{7\alpha}{9\pi t_0} \left[ \ln^2\left(\frac{k m_e E}{E_0 m_\mu}\right) + C \right] \quad (12)$$

$$M \approx \frac{7\alpha T}{9\pi} \left[ \ln^2\left(\frac{k m_e E_\mu}{E_0 m_\mu}\right) + C \right] \quad (13)$$

and for bremsstrahlung process the total number of cascades above the threshold energy  $E_0$  can be calculated by:

$$M \approx \frac{4T}{3n_{at}t_0} \ln\left(\frac{E_\mu}{E_0}\right) \quad (14)$$

$$M \approx \frac{4AT}{3N_{av}\rho t_0} \ln\left(\frac{E_\mu}{E_0}\right) \quad (15)$$

All calculations have been done for the 100 kton iron detector. We have preferred the dimensions of 100 kton iron detector are 15.6 m × 15.6 m × 78 m. We have taken an average value of path-length  $T = 1000$  rl for a muon, traversing 15 m in an iron detector. The average number of muon cascades at different threshold energies has been shown by Figure 2, which indicates that the reduction in muon cascades with the increment in threshold energy. At  $E_0 = 1$  GeV and  $E_\mu = 100$  TeV there is approximately more than 70 cascades of muons in comparison to  $E_\mu = 100$  TeV at  $E_0 = 100$  GeV.

### Estimation of muon energy loss and surface muon energy

As muon traverses through the rock between the earth's surface and detector, it produces energy losses. These losses have been originated by means of ionization, bremsstrahlung, pair production and photo nuclear processes. They can be effectively parametrized by [6,12-14] for the muons at higher energy range from [1T eV -100000T eV]. For high energy muons at depth, the discrete energy losses become more important which are mainly bremsstrahlung, pair production and photo nuclear processes. Due to these processes a calculation of muon energy loss is required to correlate the muon energies at detector level with their surface energies.

Since the average energy loss with respect to depth is directly proportional to the muon energy. Therefore the total muon energy loss is:

$$\frac{dE_\mu}{dX} = -\alpha - \beta E_\mu \quad (16)$$

where  $\alpha$  is the contribution in energy loss due to the ionization and  $\beta$  is the contribution in energy loss comes from bremsstrahlung, pair-production, photo nuclear processes i.e.,

$$\beta \rightarrow \beta_{br} + \beta_{pair} + \beta_{ph}$$

The average muon energy at detector level on traversing a distance  $x$ :

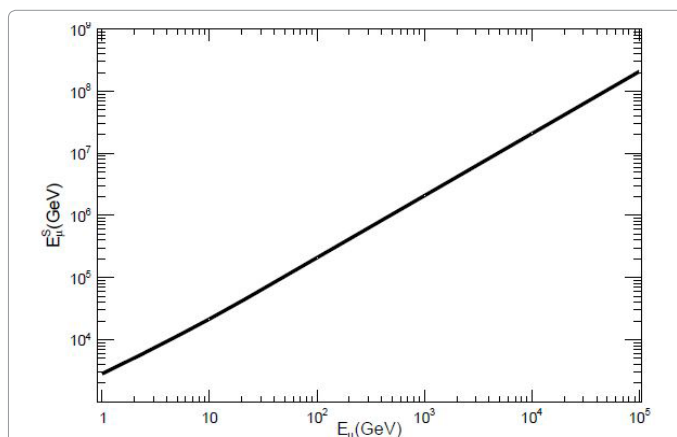


Figure 3: Muon energy  $E_\mu$  at detector level vs. surface muon energy  $E_\mu^s$ . Here we are taking the depth of the detector is  $1.89 \times 10^5 \text{g/cm}^2$ .

$$\langle E_\mu(X) \rangle = (E_\mu^s + \frac{\alpha}{\beta})e^{-\beta X} - \frac{\alpha}{\beta} \quad (17)$$

where  $E_\mu^s$  is the surface muon energy.

From equation (17) we get the relation between surface muon energy and muon energy which traverse depth  $X$

through the rock is:

$$E_\mu^s = (E_\mu + \frac{\alpha}{\beta})e^{\beta X} - \frac{\alpha}{\beta} \quad (18)$$

From equation (18) the minimum surface energy can be calculated by assuming muon energy  $E_\mu \approx 0$

$$E_{\mu(\min)}^s = \frac{\alpha}{\beta}(e^{\beta X} - 1) \quad (19)$$

The differential flux relation of muon traversing through the rock at a depth  $X$  is obtained by using the (18)

$$\frac{dN}{E_\mu^s} = \frac{dN}{dE_\mu} e^{-\beta X} \quad (20)$$

Where  $\frac{dN}{dE_\mu^s}$  is the surface muon flux having surface muon energy  $E_\mu^s$

For a depth of  $1.89 \times 10^5 \text{g/cm}^2$  the analytical value of  $\alpha$  and  $\beta$  for standard rock is parameterized by

$$\beta = 3.92 \times 10^{-6} \text{ cm}^2 / \text{g}, \frac{\alpha}{\beta} = 684 \text{ GeV} \quad (21)$$

Figure 3 shows the surface muon energy  $E_\mu^s$  corresponding to the degrade muon energy  $E_\mu$  by considering the losses. The muon traverses through the rock and entering in the detector having energy  $E_\mu$ , therefore we can calculate surface muon energy with the help of equation (18) by calculating the loss parameters. Typically through our calculations surface muon energy lies in the range of  $E_\mu^s = (2-3) \times E_\mu \text{ TeV}$

### Conventional and prompt muon fluxes

As we have mentioned earlier in introduction part of this paper that we are looking for the generation of new particle having mass (nearly GeV) at knee by the means of which we will be able to explain the changes in the spectrum. For this purpose, we have taken two flux models TIG and PRS for the conventional and prompt muon flux calculations (Figures 4 and 5) [7-11].

#### TIG model

The differential equation of conventional and prompt muon fluxes have been given by the expression as

$$\text{flux} = \frac{N_0 E^{-\gamma-1}}{1 + AE}, \quad \text{for } E < E_0 \quad (22)$$

and

$$\text{flux} = \frac{N_0' E^{-\gamma'-1}}{1 + AE}, \quad \text{for } E > E_0 \quad (23)$$

For the conventional and prompt muon fluxes, we have used the some fixed values which have been given by table [9].

### PRS model

With the help of this model we have calculated the prompt muon fluxes. This model involves the choices of the different parton distribution functions (PDF's), factorization and re-normalisation scales which results three fluxes PRS1, PRS2 and PRS3. These are the parametrised by the given formula [10].

$$\log(E_\mu^3 \times \text{flux}) = (-a + bx + cx^2 - dx^3) \quad (24)$$

Where  $x = \log(E/\text{TeV})$

The values of other PDF's and re-normalization scales have been given by the following tables (Tables 1 and 2). By using these flux models we have calculated the surface muon fluxes as well as muon fluxes at underground level. The plot 4 and plot 5 shows the renormalized surface muon fluxes and muon fluxes respectively by considering the depth:

$$X = 1.89 \times 10^5 \text{cm}^{-2}\text{g.}$$

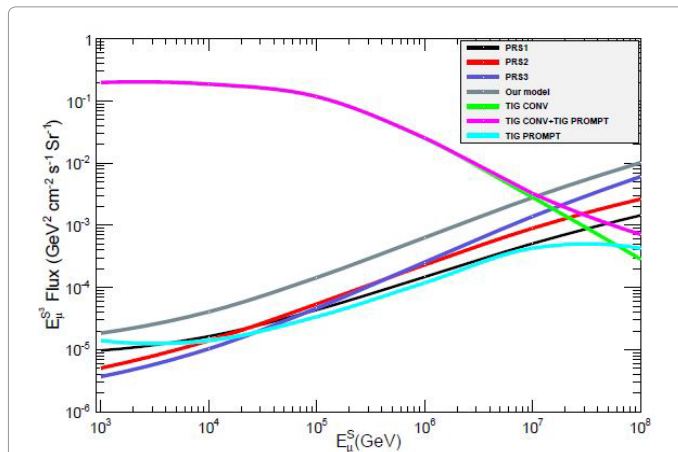


**Figure 4:**  $E_\mu^s$  flux vs. surface muon energy ( $E_\mu^s$ ) for muons entering in the underground detector by traversing through the rock of distance  $1.89 \times 10^5 \text{cm}^{-2}\text{g}$ . This figure shows the theoretically calculated normalized fluxes of muons by using different flux models-TIG conv (Green), TIG Prompt (Sky blue), TIG (conv + prompt) (Pink), PRS1 (Black), PRS2 (Red), PRS3 (Blue) and our model (Gray).

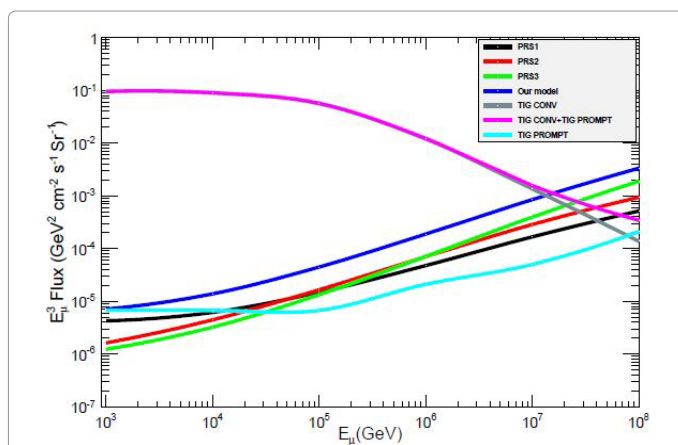


**Figure 5:**  $E_\mu^s \times \text{flux}$  vs. muon energy  $E_\mu$  has been plotted by using different flux models-TIG conv (Gray), TIG Prompt (Sky blue), TIG (Conv + prompt) (Pink), Prompt muon fluxes of PRS family-PRS1 (Black), PRS2 (Red), PRS3 (Green) and our model (Blue).

Flux	$N_0$	$N'_0$	$\gamma$	$\gamma'$	A	$E_0$
Conventional flux	0.2	0.21	1.74	2.1	$7.0 \times 10^{-3}$	$5.3 \times 10^5$
Prompt flux	$1.4 \times 10^{-5}$	$4.3 \times 10^{-4}$	1.77	2.01	$2.8 \times 10^{-8}$	$9.1 \times 10^5$

**Table 1:** The parameter of TIG model has been given by this table for conventional and prompts both Muon fluxes.

Flux model	PDF	Re-normalization scales	a	b	c	d
PRS1	CTEQ3	$M = \mu = mc$	5.37	0.0191	0.156	0.0153
PRS2	CTEQ3	$M = 2\mu = 2mc$	5.79	0.345	0.105	0.0127
PRS3	D	$M = 2\mu = 2mc$	5.91	0.290	0.143	0.0147
Our model	CTEQ3	$M = 2\mu = 2mc$	5.57	0.258	0.135	0.0132

**Table 2:** The parameters of PRS models have been given by this table. The factorization renormalizations scales are a, b, c, d are given. This gives the muon as well as anti-muon fluxes also, where mass of charm quark is shown by mc.

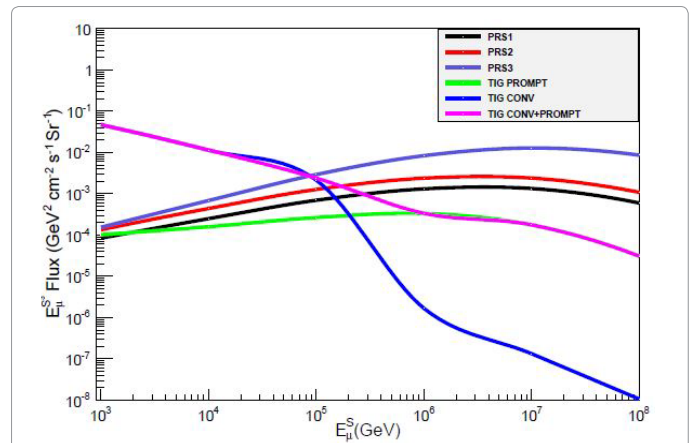


**Figure 6:**  $E_\mu^s3$  flux vs. surface muon energy ( $E_\mu^s$ ) for muons at slant depth ( $X = 3 \text{km.w.e.}$ ) entering in the under-ground detector by traversing through the rock. This figure shows the theoretically calculated normalized fluxes of muons by using different flux models- TIG conv (Light blue), TIG Prompt (Green), TIG (conv+prompt) (Pink), PRS1 (Black), PRS2 (Red) and PRS3 (Dark blue).

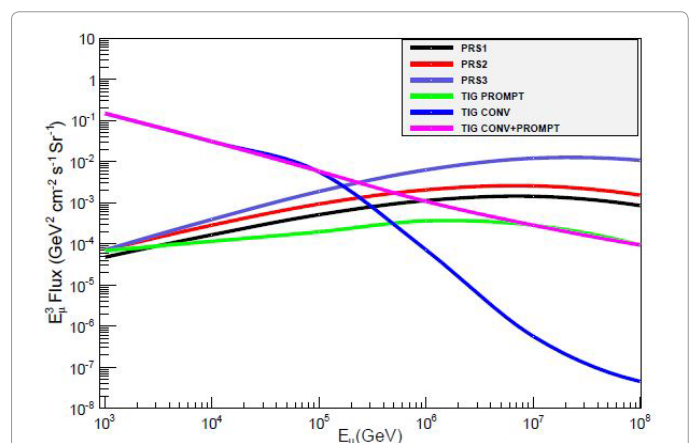


**Figure 7:**  $E_\mu^3 \times \text{flux}$  vs. muon energy  $E_\mu$  has been plotted by using different flux models-TIG conv (Light blue), TIG Prompt (Green), TIG (Conv + prompt) (Pink), PRS1 (Black), PRS2 (Red) and PRS3 (Dark blue). Figure shows the muon fluxes at slant depth ( $X = 3 \text{ km.w.e.}$ ).

On seeing these plots we may conclude that the fluxes of prompt muons cross the conventional muon fluxes beyond  $10^4 \text{TeV}$  muon energy.

### Conventional and prompt muon fluxes at slant depth

The topography of the rock for an iron detector gives the slant depth. Basically it is calculated by:

$$X(\theta) = \frac{h_0 \sec \theta}{1 + w_0 \sin \theta} \quad (25)$$

Where  $w_0$  is the slope of the rock.

Here we have used the rock density  $\rho = 2.75 \text{ gmcm}^{-3}$ . The surface muon fluxes and muon fluxes at slant depth has shown by Figures 6 and 7 respectively and can be calculated by the given parameterised formula of particular model discussed in section 7.

### Calculation of event rates

We are using iron calorimeter detector. The number of event rate above a threshold energy entering in the iron detector over five years is given by:

$$\text{Event rate}(n_\mu) = \int_{E_{th}}^{\infty} \sigma_i(E, \epsilon_0) \times \text{flux} \times \rho \times A \times T \times t \quad (26)$$

where A is the exposed area of the detector having the value  $2.4 \times 10^7 \text{ cm}^2$ .

This is given by the Table 3 which shows a large variation in the

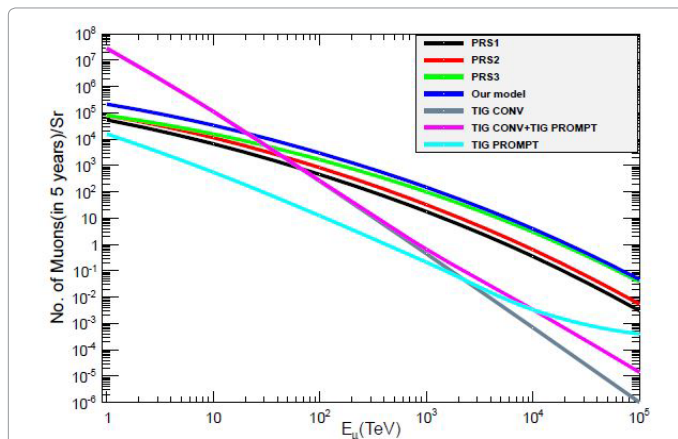


Figure 8: The figure shows number of muons vs. muon energy entering in the detector for five years of exposure time of 100 KT detectors per steradians. The surrounding effect of rock are taken into account. PRS1 (Black), PRS2 (Red), PRS3 (Green), TIG conv (Gray), TIG prompt (Sky blue), TIG (conv + prompt) (Pink), our model (Blue).

events rates which generates due to uncertainties in the muon fluxes at higher energy ranges. We may see from the Table 3 at energy 1 TeV we obtain an observable number of muons and as we are moving towards the higher energies we will get 2-3 muons only.

### Results and Discussion

We have calculated the event rates by using two different models for five years of exposer time of iron detector. The results of this calculation have been shown by the Figure 8 and tabulated our data in Table 3. We see from Table 3 that at lowest energy range i.e., at 1 TeV, the event rate is very high for five years of exposer time of detector and as we move towards the higher energy ranges at 100000 TeV; we will be unable to obtain an observable number of event rate. We have also calculated cascade numbers of muon by using equation 11 at different-2 threshold energies i.e.,  $E_0 = 5, 10, 50, 100, 300, 500, 1000, 5000, 10000, 50000 \text{ GeV}$  respectively which has tabulated in Table 4. Here we have used two flux models TIG and PRS and both flux models have based on the perturbation QCD values but they differ in their event rates. A great variation occurs in similar perterbative QCD based models PRS1, PRS2, PRS3 and our model too. Hence muon event rate produces a large uncertainties in the prediction of QCD models (i.e., charm production), which helps us to understand about the produced spectral changes in the cosmic ray at knee.

### Conclusion

In this work we have attempted to study the vertical flux of ultra-high energy cosmic ray muons at surface as well as underground at detector level. We have presented our main results in Figures 2 and 8 and Tables 3 and 4. From these results, we have obtained significantly larger muon fluxes than TIG [9] and PRS [10]. The dominance behaviour of prompt muon flux can be seen above  $10^2 \text{ TeV}$  by Figures 4-7. Hence we may conclude that the underground muon energy measurements for an energy range  $E_\mu$  from 1-10000 TeV are possible with 100 kton iron detector running over 5 years. This will give a better deal on the ultra-high energy muon fluxes in between the range of several TeV to 10 PeV. This will reduce the uncertainties present in charm production models and it will be also helps us to improve our knowledge about the ultra-high energy neutrino astronomy. In our results we have discussed the observable muon energy range 1 - 10000 TeV, which is crucial of the origin of knee. In this process our calculations of muon fluxes with and without slant depth show feasible demonstration to get deeper knowledge about the knee origin. In this paper in the first place we want to demonstrate the observational feasibility in comparison with the precise prediction through our calculation of muon measurement. Thus our results help to know more about cosmic ray physics, ultra-high energy neutrino astronomy and charm production models.

$E_\mu$ (T eV)	No. of muons in 5 years of exposer time						
	Conv. + T IG	Conv.	TIG	PRS1	PRS2	PRS3	Our model
1	$2.84 \times 10^7$	$2.87 \times 10^7$	15911	54145	79925	80479	214578
10	113204	112530	558.5	6671	11434	15784	33890
50	1672.5	1632.5	40.05	1081	1945	3483	6509
100	264.2	252	12.32	456	828.6	1672	2956
500	3.8	3.06	0.74	50.4	92.2	248	391
800	1.2	0.83	0.32	25.03	45.8	135	205
1000	0.6	0.4	0.2	17.8	32.5	99.4	149
5000	0.016	0.0049	0.01	1.25	2.2	9	13
10000	0.0034	0.0007	0.0032	0.3	0.63	3	4
50000	0.000081	$7.3 \times 10^{-6}$	0.0023	0.014	0.025	0.16	0.1
100000	0.000014	$1.01 \times 10^{-6}$	0.0004	0.003	0.0054	0.038	0.047

Table 3: Number of events of muons per solid angle for 5 years of exposure time of 100 KT iron detector by using two different models for different muon energies  $E_\mu$  (in TeV).

E (TeV)	values	1	5	10	50	100	300	500	1000	5000	10000	50000
1	2.82	11.03	3.09	2.58	-	-	-	-	-	-	-	-
10	21.55	38.73	17.35	11.03	3.09	2.6	-	-	-	-	-	-
50	104.79	69.52	38.73	28.37	11.03	6.5	2.79	2.58	-	-	-	-
100	208.84	85.68	50.83	38.73	17.35	11	4.59	3.09	2.58	-	-	-
500	1041.24	129.92	85.68	69.52	38.73	28	15.51	11.03	6.46	2.58	-	-
800	1665.54	144.61	97.63	80.29	46.75	35	20.48	15.12	9.36	2.74	-	-
1000	2081.74	151.87	103.58	85.68	50.84	39	23.12	17.35	11	3.09	2.58	-
5000	10405.74	209.57	151.87	129.9	85.68	70	47.49	38.73	28.4	11.03	6.46	2.58
10000	20810.74	237.31	175.56	151.9	103.6	86	60.89	50.84	38.7	17.35	11.03	3.09
50000	104050.7	308.45	237.31	209.6	151.9	130	98.7	85.68	69.5	38.73	28.37	11.03
100000	208100.7	341.99	266.8	342	175.6	152	117.9	103.6	85.7	50.83	38.73	17.35

**Table 4:** Number of muons cascades at different threshold energies  $E_0$  in GeV. Muon energy  $E_\mu$  is taken into TeV and  $E_s$  is the corresponding surface muon energy calculated by using the degraded muon energy by taking the depth of the rock at the surface of earth is  $1.866 \times 10^5$  g/cm<sup>2</sup>.

### Acknowledgement

The author Sharda Pandey would like to thank my co-worker for the wonderful supervision and giving a support to this work.

### References

- Gaisser TK (1990) Cosmic rays and particle physics. Cambridge University Press, Cambridge.
- Stanev T (2003) High energy cosmic rays. Springer-Praxis, Berlin.
- Panda S, Sinegovsky SI (2008) The role of polarized positrons and electrons in revealing fundamental interactions at the Linear Collider.
- Gandhi R, Panda S (2006) Probing very high energy prompt muon and neutrino fluxes and the cosmic ray knee via underground muons. Cornell University Library. Nucl Phys Proc Suppl. 91, 453.
- Bertaina M, Tsukuba V (2003) Cosmic ray transport in the galaxy. Cosmic rays p: 115.
- Gaisser T, Halzen F, Stanev T (1995) Particle physics with high energy neutrinos. Phys Rept. 258: 173-236.
- Sinegovskaya TS, Sinegeovsky SI (2001) Phys Rev D 63, 096004.
- Lipari P (1993) Lepton spectra in the earth atmosphere. Astropart Phys. 1:195-227.
- Thunman M, Ingelman G, Gondolo P (1995) Charm production and high energy atmospheric muon and neutrino fluxes. Astropart. Phys 5: 309-332.
- Pasquali L, Reno MH, Sarcevic I (1999) Lepton fluxes from atmospheric charm. Phys Rev. D59, 034020.
- Gelmini G, Gondolo P, Varieschi G (2000) Phys Rev D61, 036005, Ibid. Phys. Rev. D61, 056011.
- Kokoulin RP, Petrukhin AA (1990) Use of the big liquid argon spectrometer BARS for neutrino and cosmic-ray studies. Sov J Part Nucl 21(3): 332.
- Kokoulin RP, Petrukhin AA (1988) Nuclear instruments and methods in physics. Phys Res. A 263: 468.
- Gandhi R (2000) Probing very high energy prompts muon and neutrino fluxes and the cosmic ray knee via underground muons.